The Scientific Temper (2024) Vol. 15 (2): 2390-2396
E-ISSN: 2231-6396, ISSN: 0976-8653
Doi: 10.58414/SCIENTIFICTEMPER.2024.15.2.56
https://scientifictemper.com/

RESEARCH ARTICLE

Synthesis and characterization of pure and magnesium ion doped CPPD nanoparticles

Sonal R. Vasant

Abstract

One kind of calcium phosphate is calcium pyrophosphate, a biomaterial with a well-known bio-efficiency and a composition like that of bone mineral. It is the most often used mineral family in businesses and research about biomedicine. Calcium phosphates are the most crucial inorganic element found in physiologically hard tissues in living things. Doping with different trace elements may significantly change bone healing material's biological properties, mineralization, and early degradability. The substitution of cations in the apatite structure to mimic genuine bone, such as K^+, Na^+, Zn^{2+}, Mn^{2+} and $Mg^{2+,}$ has received significant interest. The purpose of doing this is to benefit from these cations' functions in catalysis, affecting biological activity and bone metabolism. The fourth most common cation in the human body is magnesium ion (Mg^{2+}), with a weight percentage (wt%) ranging from 0.44 to 1.23. It is one of the most significant bivalent ions. Calcium pyrophosphate dihydrate (CPPD) nanoparticles that were pure and magnesium ion doped were created using a surfactant-mediated technique. There were four different molar ratios of magnesium to calcium: 0% (Pure CPP), 2, 5, and 10%. The energy dispersive analysis of X-rays (EDAX) study confirmed the effectiveness of the doping. The materials' nanostructure was verified using transmission electron microscopy (TEM) analysis and Scherrer's formula for powder XRD signals. Fourier transfer infrared (FTIR) spectra showed that the structure had a variety of bond types. The use of thermogravimetric analysis (TGA) determined the dihydrate nature of the drug. A discussion of the results takes place.

Keywords: Bio-efficiency, Degradability, Surfactant mediated, Powder XRD, TEM, FTIR, TGA.

Introduction

Calcium phosphate (CaP) has been the most significant mineral family exploited in biomedical research and business. Researchers have attempted to create CaP materials with well-defined structures [Dorozhkin *et al.,* 2002; Vallet-Regi *et al.,* 2011]. CaP has compositions similar to bone mineral ones and is generally acknowledged for its bio-efficiency. Within living organisms, the CaPs are the inorganic elements considered the most significant in their importance is reported [Xu *et al.,* 2006]. These materials have a particular position in biomaterials because they comprise the mineral component of teeth and bones [Groot 1989; Kitsugi *et al.,* 1993; Klein *et al.,* 1984; Klein *et al.,* 1994; Klein *et al.,*1994]. Doping with different trace elements may significantly change bone healing material's biological properties, mineralization, and early degradability. Much research has focused on creating artificial bone by altering the apatite structure to include cations such as K^+, Na^+, Zn^{2+}, Mn^{2+}, and Mg^{2+} [Ito *et al.,* 2019; Miao *et al.,* 2005; Miyaji *et al.,* 2005, Izabela *et al.,* 2005]. The purpose of doing this is to benefit from these cations' functions in catalysis, affecting biological activity and bone metabolism. It has been shown that doped ions may considerably increase the degradability and mineralization of calcium pyrophosphate (CPP). These ions have an analogous positive charge to Ca^{2+} and a lower ionic radius. However, in contrast to Ca^{2+}, doped ions have an equivalent ionic radius and a more comprehensive range of positive charges, which contribute less to the degradability and mineralization of CPP and may even reverse the effects of Ca^{2+} in some situations [Song *et al.,* 2009].

Since it is one of the bivalent ions most crucial for sustaining bone health, magnesium (Mg) has attracted much interest from scientists. For example, with a weight percentage (wt %) ranging from 0.44 to 1.23 [Qi *et al.,*2008], it is one of the most abundant cations in the human body

Department of Humanities and Sciences, L.E. College, Morbi-2, Gujarat, India

***Corresponding Author:** Sonal R. Vasant, Department of Humanities and Sciences, L.E. College, Morbi-2, Gujarat, India, E-Mail: sonalvasant@iaar.co

How to cite this article: Vasant, S. R. (2024). Synthesis and characterization of pure and magnesium ion doped CPPD nanoparticles. The Scientific Temper, **15**(2):2390-2396.

Doi: 10.58414/SCIENTIFICTEMPER.2024.15.2.56

Source of support: Nil

Conflict of interest: None.

Received: 04/04/2024 **Accepted:** 05/05/2024 **Published** : 29/06/2024

and one of the most significant bivalent ions in biological apatite [Cacciotti *et al.,*2009]. Bone tissue contains between 50 to 65% of the total amount of magnesium. In contrast, the extracellular fluid contains just 1% of the magnesium [Rude *et al.,*2004; Okuma 2001]. The second most common intracellular cation is magnesium. Magnesium is essential for creating bone tissue and for the early development of bone tissue [Sogoa *et al.,* 2004]. Furthermore, magnesium directly stimulates osteoblast proliferation and indirectly affects bone resorption, having a similar impact to insulin, a growth factor known to be connected to osteoblasts [Serre *et al.,* 1998; Suchanek *et al.,* 2004]. The percentage of magnesium in enamel, dentin, and bone is 0.44, 1.23, and 0.72%, respectively. [Suchanek *et al.,* 2004]. Its presence suppresses the growth and activity of osteoblast-like cells, hinders crystallization, and diminishes the size of the crystals [Sun *et al.,* 2010; Bigi *et al.,* 1993; TenHuisen and Brown, 1997; LeGeros, 1991]. On the flip side, it affects all steps of skeletal metabolism when missing, leading to decreased osteoblastic and osteoclastic activity, brittle bone, and a halt to bone growth [Percival 1999, Yasukawa *et al.,* 1996, Okazaki 1991, Kim *et al.,* 2003]. Magnesium ions must be present for over 100 enzymes to be catalytically active. All enzymes that use or produce adenosine-5-triphosphate (ATP) fall within this category. These ion-doped materials exhibit no toxicity and do not harm the surrounding environment throughout the CPP breakdown process. Moreover, they may significantly impact bone metabolism, growth, and food absorption [Christoffersen *et al.,* 1997; Zreiqat *et al.,* 2002; Ito, 2005; Zhang *et al.,* 2005]. Many studies have focused on hydroxyapatite doped with magnesium ions [Qi *et al.,* 2008; Laurencin *et al.,* 2011], TCP [Lee *et al.,* 2009; Gozalian *et al.,* 2011], biphasic CaPs [Gomes *et al.,* 2009; Marchia *et al.,* 2007; Bose *et al.,* 2013], and CPP [Masala *et al.,* 2003].

The geometrical considerations, such as the disparity in ionic radii (around 0.3 Å difference in radius according to the Pauling scale) and the improved electrostatic stability, make the replacement of Mg^{2+} ions in CaPs the favored option [Mayer *et al.,* 1997]. This is because Ca^{2+} has an ionic radius of 0.99 Å, whereas Mg^{2+} has a much lower ionic radius of 0.69 Å [Shannon 1976]. The modifying ion will be absorbed into the CaP structure relatively quickly because it has an electrical charge and ionic radius similar to the Ca^{2+} ion. The present study used a surfactant-mediated approach to produce Mg-ion-doped CPPD nanoparticles. After that, these nanoparticles were examined using various instruments, such as powder XRD, TEM, FTIR, EDAX, and TGA. This was carried out with consideration for the many applications of Mg-ion-doped CaPs.

Experimental Technique

The production of CaPs doped with magnesium ions has been attempted by several researchers using a variety of methods, including precipitation [Sader, 2009; Kannan *et al.,* 2007; Kubarev *et al.,* 2008; Landi *et al.,* 2006], wet mixing [Zyman *et al.,* 2006; Tan *et al.,* 2008], solid-state processes [Tardei *et al.,* 2006], and the sol-gel approach [Toibah *et al.,* 2008]. The first components used were Triton X-100, AR-grade calcium nitrate tetrahydrate, magnesium chloride, and sodium pyrophosphate. To make Mg ion doped CPPD, aqueous solutions of magnesium chloride and calcium nitrate tetrahydrate $Ca(NO_3)_2.4H_2O$ were combined in a range of 2 to 10% magnesium to calcium by mass. Next, a non-ionic surfactant called Triton X-100 was added to the mixture in a way that kept the water-to-surfactant ratio constant at 5:1. The combination of $Ca(NO)_3)_2.4H_2O$, $MgCl_2$, and surfactant was gradually added to the sodium pyrophosphate ($Na_4P_2O_7$) aqueous solution at a concentration of 0.25 M while stirring constantly at 50°C. The ensuing stoichiometric reaction is anticipated to take place:

$$2Na_4P_2O_7 + 4(Ca(NO_3)_2.4H_2O) + 2(MgCl_2) \rightarrow$$
$$2(Ca_{2-x}Mg_xP_2O_7.2H_2O) + 8(NaNO_3) + 2Ca_xMg_{2-x}Cl_2 + 12H_2O$$

The subsequent steps were rapid filtering, rinsing with deionized water to remove surfactant, and then air drying of the precipitates. The end product was obtained in powder form.

Result and Analysis

Energy Dispersive Analysis of X-rays (EDAX)

Magnesium ions were found in the sample, according to the results of the EDAX analysis, which was performed to ascertain the sample's elemental composition. Calcium, phosphorus, and oxygen were found to be the primary components of the doped samples. In contrast, magnesium was found to be a very minute amount. The doping technique was also successful since the magnesium-to-calcium molar ratio increased with the magnesium amount. The wt% of magnesium attained for 2, 5, and 10% doped CPPD nanoparticles was found to be 1.19, 1.59, and 3.40, respectively. This was discovered via the process of synthesis. Compared to what was predicted, magnesium ion concentration is much lower. The initial ionization energies, 590 kJ/mole for calcium and 736 kJ/mole for magnesium, may explain this phenomenon. Due to this observation, calcium's chemical reactivity is higher than magnesium's [Dickerson *et al.,* 1979]. $Ca_{1.83}Mg_{0.17}P_2O_7.2H_2O$, $Ca_{1.75}Mg_{0.49}P_2O_7.2H_2O$, and $Ca_{1.51}Mg_{0.49}P_2O_7.2H_2O$ is the stoichiometric formulae that have been presented for Mg 2, 5, and 10% doped CPPD nanoparticles, respectively, according to the results of the EDAX in their respective studies.

Powder XRD

Figure 1 compares the powder X-ray diffraction data for CPPD nanoparticles rich in magnesium ions and those that are not. The results demonstrate that the two nanoparticle kinds have distinct impacts. The unit cell parameters of the triclinic system of pure CPPD nanoparticles are as follows: a =

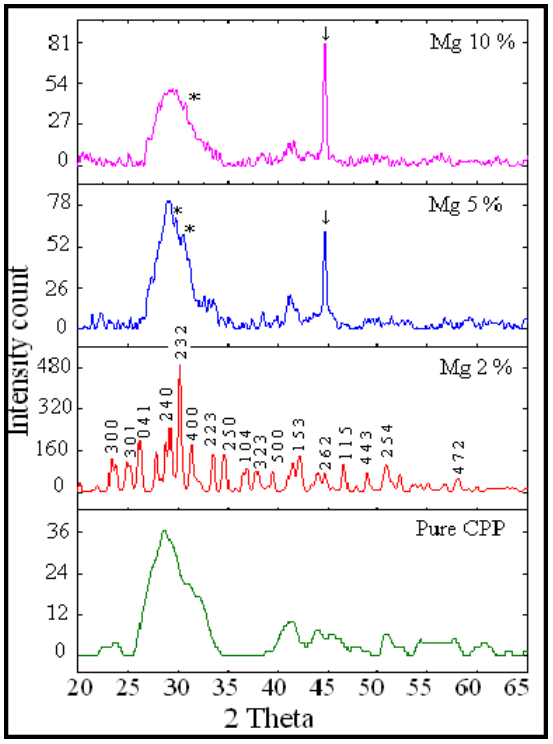

Figure 1: XRD patterns for pure and Mg ion doped CPPD nanoparticles

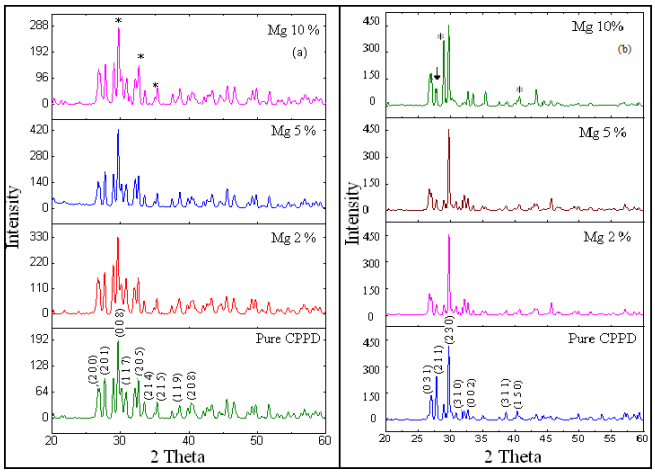

Figure 2: XRD patterns for pure and Mg ion doped CPPD Nanoparticles calcined at (a) 900°C and (b) 1250°C

7.365 Å, b = 8.287 Å, c = 6.691 Å, α = 102.96 °, β = 72.73°, and γ = 95.01°. The features of the triclinic system specify these traits. These values are considered acceptable as they align with the values given in the literature (JCPDS No. 28-0233).

With unit cell parameters of a = 11.44 Å, b = 14.47 Å, and c = 9.97 Å (JCPDS No. 41-0490), the sample of CPPD nanoparticles that have been doped with magnesium ions exhibits an orthorhombic structure. Furthermore, the sample is exceptionally crystalline in its natural state. The (1 0 1) plane of $Ca_2Mg(PO_4)_2.2H_2O$ (JCPDS No. 26-1063) overlaps the most incredible reflection of CPPD (3 0 2) at 29.21^0 (d= 3.04 Å). This reflection is the strongest of the three planes-the distinctive peaks of $Ca_2Mg(PO_4)_2.2H_2O$. The symbol in Figure 1 represents the same. These reflections occur at d = 3.04 Å(29.21°) and 3.02 Å(29.57°) in CPPD doped with 2 and 10% magnesium ions, respectively. As illustrated by the little arrow, the intense peak found at about 44.5° in Mg 5 and 10% doped CPPD may result from unreacted $MgCl_2$. On the other hand, the crystallinity diminishes when the concentration of magnesium ions in the doping concentrate grows to 5 and 10%. This result is in consistent with the reported one [LeGeros 1983, LeGeros 1984 and Okazaki *et al.,* 1986].

The samples were calcined at 900°C for an hour to determine the phases in a muffle furnace while within ceramic crucibles. Powder X-ray diffraction was then used to determine the phases. This examined the potential for a phase change at higher temperatures. Figure 2(a) displays the powder XRD patterns of CPPD calcined at 900°C, pure and doped with magnesium ions. The JCPDS No. 20-0024 data clearly shows that the pure CPPD sample displays every β-CPPP reflection on a tetragonal crystal structure. Further information on the unit cell characteristics is provided by a = b = 6.684 Å and c = 24.145 Å, respectively.

The intensity of various peaks having d-spacing values 3.01 *Å* (29.67°), 2.79 Å (32.12°), 2.74 Å (32.55°) and 2.67 Å (33.42°) It has been discovered that the distinctive peaks of $Ca_{2.81}Mg_{0.19}(PO_4)_2$ (JCPDS No. 70-0682) are becoming more prominent as the concentration of magnesium ions in the doping process rises. The symbols * indicate these peaks in Figure 2(a).

The Mg ion-doped CPPD nanoparticles were calcined to 1250°C by placing them in ceramic crucibles and heating them in a muffle furnace for fifteen minutes. Figure 2(b) shows an illustration of the powder XRD patterns. All the usual reflections of orthorhombic-structured α-calcium pyrophosphate (CPP) were seen on the powder X-ray diffraction (XRD) pattern of pure CPPD (JCPDS No. 09-0345).

As the doping concentration is raised, it is seen that the intensity of distinct peaks with d-spacing values of 3.04 Å (29.21°) and 3.01 Å (29.67°) increases. These are the typical peaks of $Ca_{2.81}Mg_{0.19}(PO_4)_2$ (JCPDS No. 70-0682), as previously mentioned. A directional arrow may be seen in Figure 2(b) to indicate the peaks.

An effort was made to compute the average particle size using Scherrer's formula. The results showed that the average particle size for pure CPPD was 4 nm. The average particle size for calcined CPPD at 900 and 1250°C was 76 nm and 119 nm, respectively. Table 1 compiles the crystallite size measurements obtained for the synthesized and calcined samples. It is possible to hypothesize that the 2% magnesium ion doping may be a substitutional one with a lower ionic radius and contribute to better crystallite order achievement.

On the other hand, the larger quantity of doping further brings about distortion in the unit cell and further

Table 1: Values of average crystallite size and strain for pure and Mg-ion doped CPPD nanoparticles

Samples	*Average crystallite size Scherrer's formula (nm)*			*Average crystallite size Williamson-Hall (nm)*			*Strain ×10^{-03}*		
	As syn- the-sized	*900 °C*	*1250 °C*	*As syn- the-Sized*	*900 °C*	*1250 °C*	*As syn- the-sized*	*900 °C*	*1250 °C*
CPPD	4	76	119	12	97	121	6.1	1.3	0.4
Mg- 2% CPPD	50.60	89.54	125.6	56.4	98.31	120.3	1.4	1.1	0.6
Mg- 5% CPPD	10.2	93.57	122.1	13.6	95.68	118.9	4.8	1.4	0.3
Mg-10% CPPD	4.2	93.20	119.20	9.3	99.39	116.7	5.6	1.1	0.5

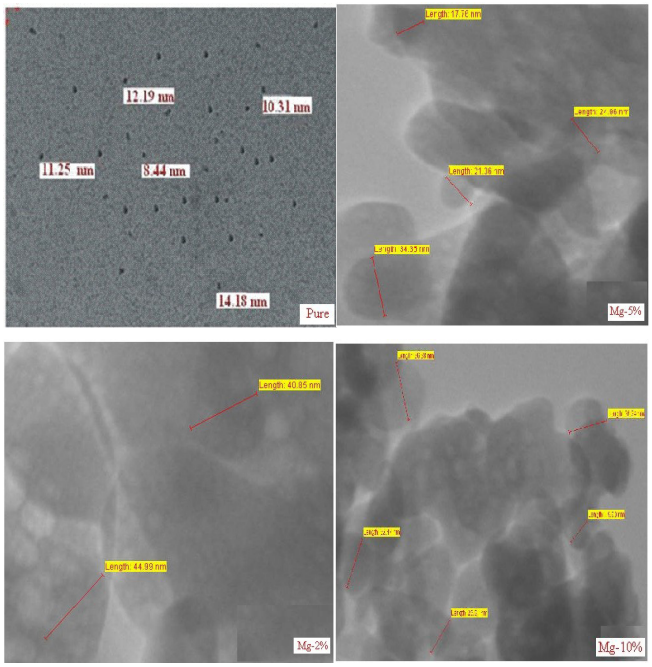

Figure 3: TEM images for pure and Mg ion doped CPPD nanoparticles

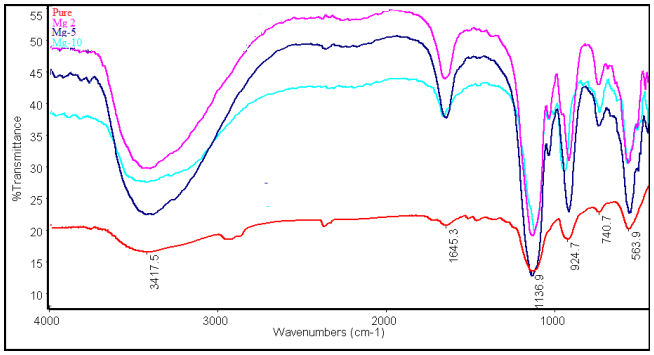

Figure 4: FTIR spectra of pure and Mg ion doped CPPD nanoparticles

contributes to the loss of crystallinity. This nature is shown by the larger values of average particle size for 2% Mg ion doped CPPD in Table 1, as well as the lower amount of strain. According to past observations, temperature has been shown to influence the crystalline phase fraction, crystallite size substantially, and, as a result, specific surface area [Lazic *et al.,* 2001]. This conclusion is compatible with those previously observed findings.

TEM Study

The application of transmission electron microscopy (TEM) allowed for the verification of the materials' form and particle size. The TEM images of both the pure and Mg-ion doped CPPD nanoparticles are shown in Figure 3. Particle sizes range from 4 to 80 nm; the pictures show these differences. Particle sizes of CPPD doped with magnesium ions at a concentration of 2% are greater than those of other doping concentrations, as demonstrated by powder X-ray diffraction data. However, the agglomerated form is seen in CPPD nanoparticles doped with 5 and 10% magnesium ions. Various authors have explained the aggregation of particles within the context of surfactants Palla and Shah, 2000, Giulietti *et al.,* 2001].

FTIR Spectroscopy

Because every substance is a one-of-a-kind collection of atoms, no two compounds will ever create an infrared spectrum that is identical to one another. Consequently, infrared spectroscopy can potentially identify (qualitatively analyze) the materials. Figure 4 illustrates the fourier transform infrared spectra of pure and magnesium ion-doped CPPD nanoparticles. Table 2 has a compilation of the assignments.

Adsorbed water's O-H stretching and plane bending vibrations are represented by two broad bands, one occurring at 1632 cm^{-1} and the other between 3670 and 3200 cm^{-1}. The P-O-P bridge and the radical $(PO_2)^{2-}$ are components of the anion $(P_2O_7)^{4-}$. The $(P_2O_7)^{4-}$ vibrational modes were seen in the 1500 to 400 cm^{-1} range, consistent with previous research [Boonchom *et al.,* 2009, Harcharras *et al.,* 2003].

TGA Study

Thermogravimetric analysis (TGA) is a method that is now in use to assess the changes in a sample's physical and chemical

Table 2: Assignments of different absorption bands in the FTIR spectra of pure and Mg-ion doped CPPD nanoparticles

Assignments	*Observed absorption (cm^{-1})*			
	Pure CPPD	*Mg- 2 % CPPD*	*Mg- 5 % CPPD*	*Mg- 10 % CPPD*
-O-H stretching vibration	3417.5	3410.8	3407.5	3411.9
-O-H plane bending vibration	1645.3	1670.8	1650.4	1642.2
Asymmetric Stretching of the $(PO_2)^{2-}$ radical	1136.9	1151.1, 1034.2	1127.4	1131.4
symmetric Stretching of the $(PO_2)^{2-}$ radical	924.7	935.3	906.7	919.0
P-O-P bridge vibrations	740.7	739.2	739.2	743.2
Metal- Oxygen stretching Vibrations	563.9	567.5	553.3	547.1

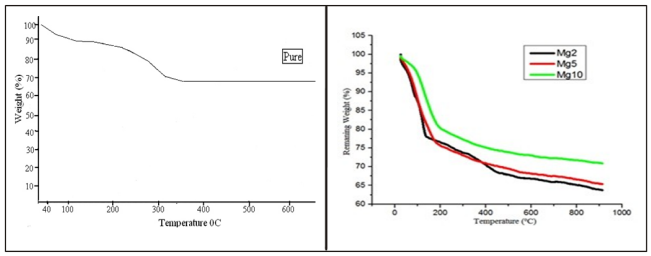

Figure 5: Thermo-grams of pure and Mg ion doped CPPD nanoparticles

Table 3: Experimentally obtained weight percent (wt %) at different temperatures for pure and Mg -ion doped CPPD nanoparticles

Substance	*Observed (wt %) at various temperatures*		
	Room temperature	*100°C*	*600°C*
Pure CPPD	100	92.32	66.87
Mg-2% CPPD	100	96.17	66.75
Mg-5% CPPD	100	95.20	68.13
Mg-10% CPPD	100	93.32	73.01

features as a temperature function. To heat the samples in the correct conditions, they are placed in an alumina crucible, and their mass change is monitored continuously. Some variables that affect the material's thermal reaction include sample volume, particle size, phase purity, and so on [Haines 1995].

Thermographic analysis of pure and Mg-ion doped CPPD nanoparticles is shown in Figure 5. The thermograms indicate that CPPD nanoparticles, pure and doped with magnesium ions, have superior thermal stability compared to other nanoparticle types. The thermogram was used to compute the water of hydration. According to the findings, around 1.79, 2.03, 1.88, and 2.1 water molecules bonded to pure, Mg-2%, 5, and 10 ion doped CPP, respectively. This demonstrated that the molecules pyrophosphate was in their dihydrate condition.

At room temperature, at 100, and 600°C, the values of the residual wt% are shown in Table 3. Since there was no discernible reduction in weight after 400°C, it was discovered that all of the samples were very stable.

An increase improved the stability in the number of magnesium ions found in the CPPD microparticles. This might result from the reduced lattice energy by substituting magnesium ions in CPPD, which has a stabilizing effect. Table 3 displays the wt% values at room temperature, 100, and 600°C for pure and Mg-ion doped CPPD nanoparticles. It is discovered that the residual wt% values rise as the doping of Mg ions increases at 600°C with increasing temperatures. Because of this, there is a lower quantity of breakdown and better thermal stability.

The stoichiometric formulae are suggested as $Ca_2P_2O_7.1.79H_2O$, $Ca_{1.83}Mg_{0.17}P_2O_7.2.03H_2O$, $Ca_{1.75}Mg_{0.49}P_2O_7.1.88H_2O$ and $Ca_{1.51}Mg_{0.49}P_2O_7.2.1H_2O$ for pure, 2, 5, and 10% Mg ion doped samples, respectively. These formulae are derived from the combination of the water molecules attached to the CPP nanoparticles doped with magnesium ions.

Conclusion

Using a surfactant-mediated approach, CPPD nanoparticles doped with magnesium ions were synthesized. Magnesium ion doping into CPPD nanoparticles was effective, according to the EDAX study. While CPPD nanoparticles doped with Mg-2% ions showed better crystallinity, pyrophosphate compounds doped with Mg-5 and 10% ions produced a broader and more distorted pattern than pure CPPD nanoparticles. Adding magnesium ions drastically changed the nanoparticle's crystallinity. The doped CPPD nanoparticles exhibited higher concentrations of the $Ca_2Mg(PO_4)_2$ $2H_2O$ reflections. The powder X-ray Diffraction (XRD) technique, which incorporates reflections of $Ca_{2.81}Mg_{0.19}(PO_4)$, demonstrated the formation of the β-CPP and α-CPP phases of CPP. A furnace was used for calcining the CPPD nanoparticles doped with Mg ions at 900 and 1250°C, respectively. The almost spherical shape of the CPPD nanoparticles doped with magnesium ions was shown by TEM. They also included particles ranging from 4 to 80 nm in size. Agglomeration was also more pronounced in the Mg ion-doped samples compared to the unadulterated CPPD nanoparticles. In pure and Mg ion-doped CPPD nanoparticles, O-H stretching and

bending vibrations, pyrophosphate functional groups, and metal-oxygen vibrations were confirmed through Fourier transform infrared spectra. Magnesium ion doped and pure nanoparticles showed enhanced thermal stability and thermograms that verified the dihydrate form. In light of the findings from EDAX and TGA, the stoichiometric equations for ion-doped pyrophosphate nanoparticles have been suggested. At 2% Mg, the formula is $Ca_{1.83}Mg_{0.17}P_2O_7$. $2.03H_2O$; at 5% Mg, it's $Ca_{1.75}Mg_{0.49}P_2O_7$.$1.88H_2O$; and at 10% Mg, it's $Ca_{1.51}Mg_{0.49}P_2O_7$. $2.1H_2O$.

Acknowledgment

Saurashtra University's Physics Department in Rajkot, India, deserves gratitude from the author. The administrations of Lukhdhirji Engineering College in Morbi and Government Engineering College in Rajkot have been very encouraging and helpful, and she is grateful to them.

References

Bigi, A., Falini, G., Foresti, E., Gazzano, M., Ripamonti, A., & Roveri, N. (1993). Magnesium and carbonate in biological hydroxyapatite. Journal of Inorganic Biochemistry, 49(1), 69-78.

Cacciotti, I., Bianco, A., Lombardi, M., & Montanaro, L. (2009). Hydroxyapatite-silicon carbide composites with high mechanical properties. Journal of the European Ceramic Society, 29(12), 2969-2978.

Christoffersen, J., Christoffersen, M. R., Kolthoff, N., & Barenholat, O. (1997). Growth kinetics of calcium phosphate crystals. Bone, 20(1), 47-54.

De Groot, K. (1989). Bioceramics consisting of calcium phosphate salts. Journal of Biomedical Materials Research, 23(11), 1367-1381.

Dorozhkin, S. V., & Epple, M. (2002). Biological and medical significance of calcium phosphates. Angewandte Chemie International Edition, 41(17), 3130-3146.

Ito, A., Kawamura, H., Miyakawa, S., Layrolle, P., Kanzaki, N., Treboux, G., Onuma, K., & Tsutsumi, S. (2001). Electrophoretic deposition of hydroxyapatite on titanium alloy for biomaterial applications. Journal of Biomedical Materials Research, 60(2), 224-232.

Ito, A., Otsuka, M., Kawamura, H., Ikeuchi, M., Ohgushi, H., Sogo, Y., & Ichinose, N. (2005). Preparation of zinc-containing hydroxyapatite and its cytocompatibility. Current Applied Physics, 5(5), 402-406.

Izabela, G., Zygmunt, M., & Bogustaw, M. (2005). Influence of zirconium on the microstructure and properties of hydroxyapatite. Journal of Biomedical Materials Research Part A, 75(4), 788-795.

Kim, S., Lee, J., Kim, Y., Riu, D. H., Jung, S., Lee, Y., Chung, S., & Kim, Y. (2003). Synthesis and characterization of hydroxyapatite nanoparticles by hydrothermal method. Biomaterials, 24(7), 1335-1341.

Kitsugi, T., Yamamuro, T., Nakamura, T., Kotani, S., Kokubo, T., & Takeuchi, H. (1993). Bone bonding behavior of titanium fiber mesh implants in dogs. Biomaterials, 14(3), 216-224.

Klein, C. P., Driessen, A. A., & De Groot, K. (1984). Biodegradation behavior of various calcium phosphate materials in bone tissue. Biomaterials, 5(3), 157-161.

Klein, C. P., Patka, P., Wolke, J. G., De Blieck-Hogervorst, J. M., & De Groot, K. (1994). Long-term in vivo study of plasma-sprayed coatings on titanium implants. Biomaterials, 15(2), 146-150.

Klein, C. P., Wolke, J. G., De Blieck-Hogervorst, J. M., & De Groot, K. (1994). Calcium phosphate plasma-sprayed coatings and their stability: an in vivo study. Journal of Biomedical Materials Research, 28(8), 961-967.

LeGeros, R. Z. (1991). Calcium Phosphates in Oral Biology and Medicine. Basel: Karger.

Miao, S., Weng, W., Cheng, K., Du, P., Shen, G., Han, G., & Zhang, S. (2005). Surface characterization of hydroxyapatite/titania composite coatings deposited by plasma spraying. Surface and Coatings Technology, 198(1-3), 223-227.

Miyaji, F., Kono, Y., & Suyama, Y. (2005). Formation of hydroxyapatite on the surface of Ti-based alloys modified with ion implantation. Materials Research Bulletin, 40(12), 209-216.

Okazaki, M. (1991). Biomaterials science: an introduction to materials in medicine. Biomaterials, 11(7), 831-835.

Okuma, T. (2001). Magnesium and bone strength. Nutrition, 17(7-8), 679-680.

Percival, M. (1999). Bone health and osteoporosis. Applied Nutritional Science Reports, 5(1), 1-10.

Qi, G., Zhang, S., Khor, K. A., Lye, S. W., Zeng, X., Weng, W., Liu, C., Venkatraman, S. S., & Ma, L. L. (2008). Characterization of bioactive glass coatings produced by a multi-step sol-gel process. Applied Surface Science, 255(5), 304-310.

Rude, R. K., & Gruber, H. E. (2004). Magnesium deficiency and osteoporosis: animal and human observations. Journal of Nutritional Biochemistry, 15(12), 710-716.

Serre, C. M., Papillard, M., Chavassieux, P., Voegel, J. C., & Boivin, G. (1998). Alendronate and bone fragility: histomorphometric analysis of biopsies from children and adults. Journal of Biomedical Materials Research, 42(4), 626-633.

Sogoa, Y., Ito, A., Kamo, M., Sakurai, T., Onuma, K., Ichinose, N., Otsuka, M., & LeGeros, R. Z. (2004). Preparation and characterization of zinc-containing hydroxyapatite powders. Materials Science and Engineering: C, 24(5), 709-712.

Song, W., Tian, M., Chen, F., Tian, Y., Wan, C., & Yu, X. (2009). Novel composites of bioactive glass and poly(lactic-co-glycolic acid) for potential bone replacement. Journal of Biomedical Materials Research Part B: Applied Biomaterials, 89(2), 430-437.

Suchanek, W. L., Byrappa, K., Shuk, P., & Riman, R. E. (2004). Mechanochemical synthesis of hydroxyapatite by room temperature hydrothermal treatment. Biomaterials, 25(19), 4647-4657.

Suchanek, W. L., Byrappa, K., Shuk, P., Riman, R. E., Janas, V. F., & TenHuisen, K. S. (2004). Mechanochemical-hydrothermal synthesis of carbonated apatite powders at room temperature. Journal of Solid State Chemistry, 177(3), 793-799.

Sun, Z. P., Ercan, B., Evis, Z., & Webster, T. J. (2010). Comparison of cytotoxicity and genotoxicity of aluminum oxide and hydroxyapatite nanoparticles. Journal of Biomedical Materials Research Part A, 94(3), 806-814.

TenHuisen, K. S., & Brown, P. W. (1997). The formation of hydroxyapatite at elevated temperatures. Journal of Biomedical Materials Research, 36(2), 306-318.

Vallet-Regí, M., & Ruiz-Hernández, E. (2011). Bioceramics: from bone

regeneration to cancer nanomedicine. Advanced Materials, 23(44), 5177-5218.

Xu, Z. P., Zeng, Q. H., Lu, G. Q., & Yu, A. B. (2006). Inorganic nanoparticles as carriers for efficient cellular delivery. Chemical Engineering Science, 61(3), 1027-1040.

Yasukawa, A., Ouchi, S., Kandori, K., & Isshikawa, T. (1996). Preparation of hydroxyapatite coatings by the sol-gel process. Journal of Materials Chemistry, 6(8), 1401-1406.

Zreiqat, H., Howlett, C. R., Zannettino, A., Evans, P., Schulze-Tanzil, G., Knabe, C., & Shakibaei, M. (2002). Mechanisms of bone growth on titanium implants. Journal of Biomedical Materials Research, 62(2), 175-184.